

Retrieval-Enhanced Visual Prompt Learning for Few-shot Classification

Jintao Rong, Hao Chen, Tianxiao Chen, Linlin Ou, Xinyi Yu, Yifan Liu

June 19, 2024

Abstract The Contrastive Language-Image Pretraining (CLIP) model has been widely used in various downstream vision tasks. To augment its capacity for these tasks, the few-shot learning paradigm has been widely adopted. However, current paradigms may struggle with fine-grained classification and satellite image recognition due to domain gaps widening. To address this limitation, we propose retrieval-enhanced visual prompt learning (RePrompt), which introduces retrieval mechanisms to cache the knowledge of downstream tasks. RePrompt constructs a retrieval database from either training examples or external data if available, and uses a retrieval mechanism to enhance multiple stages of a simple prompt learning baseline, thus narrowing the domain gap. During inference, our enhanced model can reference similar samples brought by retrieval to make more accurate predictions. A detailed analysis reveals that retrieval helps to improve the distribution of late features, thus, improving generalization for downstream tasks. RePrompt attains state-of-the-art performance on a wide range of vision datasets, including 11 image datasets, 3 video datasets, 1 multi-view dataset, and 4 domain generalization benchmarks.

Keywords few-shot learning · prompt tuning · image classification · video understanding · multi-view image classification

1 Introduction

Visual concept recognition has achieved remarkable success in closed-set scenarios with large-scale training sets, typically ImageNet dataset. The recognition accuracy can even surpass human ability. However, it may not always be feasible to have a large training set for each specific visual concept in certain downstream tasks. How to learn a robust visual concept recognition system with low-shot data has become a challenging but valuable problem in computer vision. Previous methods [1–3] mainly focus on learning a transferable visual representation from a source domain and quickly adapting to few-shot downstream tasks through fine-tuning techniques. However, limited by the categories and closed-set training samples in the source domain, these few-shot learning algorithms are only effective in impractically simple settings, such as distinguishing 5-way 1-shot classification.

Recent advancements in visual representation learning have been propelled by the emergence of large-scale vision-language models, such as CLIP [4] and ALIGN [5]. The feasibility of applying these visual language models in addressing more challenging low-shot learning problems has attracted considerable attention within the research community [4, 6–8]. In practice, it is cumbersome to fine-tune the entire vision-language model for transfer learning in each downstream task. Furthermore, finetuning the full model can result in catastrophic forgetting [9, 10], leading to poor performance on new tasks despite the pre-trained model’s initial suc-

Jintao Rong, Linlin Ou, Xinyi Yu(✉), Tianxiao Chen
College of Information Technology, ZheJiang University of
Technology
E-mail: {2111903071, linlinou, yuxy,
202006010503}@zjut.edu.cn

Hao Chen(✉)
Zhejiang University
E-mail: haochen.cad@zju.edu.cn

Yifan Liu
School of Computer Science, The University of Adelaide
E-mail: yifan.liu04@adelaide.edu.au

cess. To address these challenges, CoOP [6] first proposes a few-shot evaluation framework for visual language models. There are full C classes of downstream tasks and each class has 1/2/4/8/16-shot samples. Meanwhile, CoOP designs a learnable text prompt to replace the sub-optimal hand-crafted text prompt templates.

Nevertheless, the frozen image feature representation also leads to sub-optimal performance. Inspired by VPT [11], many studies [8, 12–15] consider adding additional learnable visual tokens into the image encoder to parameter-efficient fine-tune the vision-language models on downstream tasks. Despite significant improvements achieved by these methods for few-shot learning, these parametric models struggle to generalize to extremely low-shot data or atypical instances, often relying on rote memorization. For instance, given only one image per class, CoOP performs even worse than the zero-shot classification results of CLIP.

Retrieval-augmentation approaches [16–21] are employed to retrieve knowledge corpus and generate additional references, thereby enhancing performance in low-resource scenarios. Large Language Models (LLM) also get advancements with retrieval-augmentation approaches and further develop Retrieval Augmentation Generation (RAG) [22]. However, the application of retrieval augmentation to visual language models remains underexplored. Tip-Adapter [21], a key-value cache model, is constructed as a retrieval auxiliary classifier for CLIP. It leverages the similarity between the test and few-shot training samples, calculating affinity matrixes in text feature space and image feature space. However, it is observed that the variances and means of visual modal similarities are smaller compared to those in visual-language modalities [23]. This phenomenon is caused by CLIP maximizing the cosine similarity between paired samples in different modalities during its contrastive learning training, without considering the intra-modality similarity. Consequently, the image similarity metrics employed by Tip-Adapter, derived from CLIP, are potentially compromised by domain gaps and an insufficient adaptation to downstream datasets.

In this work, we investigate the feasibility of learning prompts from a cache model, which facilitates the enhancement of query image features to adjust image-image similarities. To simultaneously optimize these aspects, we introduce Retrieval-enhanced visual Prompt learning (RePrompt), which incorporates a retrieval mechanism for associatively learning knowledge representations from downstream tasks. RePrompt establishes a retrieval database that stores common training image representations as retrieval keys. The current image representations retrieve relevant cached knowledge from the database. Unlike Sus-X [23], which expands the re-

trieval database using external datasets like LAION [24], our method adheres strictly to the principles of few-shot learning by not utilizing external datasets. Nonetheless, our method can still benefit from incorporating external knowledge.

To integrate the retrieved knowledge into prompt learning, we consider two enhanced strategies based on the nature of the retrieved value. If the retrieved value is the common training image representation, RePrompt dynamically learns retrieval-enhanced visual prompts based on the retrieved values and inserts them into the inputs of multiple layers of the image encoder. If the retrieved value corresponds to a label, a learnable k NN classifier is applied to predict classification results. These results are linearly interpolated into the final prediction. To harmonize these strategies, we utilize a non-parametric k NN algorithm between the query instance and the database. This allows us to establish a prior distribution and construct a loss function that guides the training process.

Our experiments show that RePrompt outperforms previous methods and achieves state-of-the-art performance under various few-shot settings for 11 image datasets, 3 video datasets, and a multi-view dataset. Moreover, superior performance on 4 domain generalization benchmarks also demonstrates the generalization ability of our RePrompt for unseen domains.

In summary, the main contributions of our work include:

- We propose the design of visual Prompt learning with retrieval enhancement, called RePrompt. Specifically, we establish a retrieval database using training examples and implement retrieval-enhanced mechanisms throughout the model, including the input, middle layers, output, and training process.
- We explore the feasibility of introducing a retrieval system to augment the prompt learning for vision language models, which dynamically select relevant references during inference conditioned on the input. This strategy significantly increases the model performance on downstream few-shot classification.
- The proposed RePrompt has strong flexibility and can be easily extended to tasks other than image datasets. For instance, We extend the framework to video understanding and multi-view recognition tasks.
- The proposed RePrompt achieves state-of-the-art performance over 11 image datasets, 3 video datasets, and 1 multi-view image dataset, under various few-shot settings. It also demonstrates superior performance on 4 domain generalization benchmarks.
- We further summarize the patterns between the properties of external memory and retrieval enhance-

ment mechanisms, which will contribute to a better understanding of retrieval enhancement methods in the academic community.

2 Related Work

Retrieval-augmented models have gained significant attention in the fields of Natural Language Processing (NLP) and Computer Vision (CV). Numerous studies have augmented large language models with external memory through retrieval-enhancement mechanism [17–19, 25–27]. The integration of knowledge into a language model involves retrieving relevant samples from external memory, thereby enabling the model to generate more informed predictions based on these samples. Typically, the external memory comprises a collection of text paragraphs or a structured knowledge base. The BERT-kNN model [26] combines the outputs of a trained BERT model with a non-parametric k NN model for question answering tasks. REALM [19] acquires external knowledge from Wikipedia. Karpukhin et al. [25] developed a dense passage retrieval system for open-domain question answering. RETRO [17] demonstrates how to blend retrieved tokens with input tokens in a transformer architecture and methodically evaluates the influence of large-scale external memory datasets on NLP tasks. Chen et al. [18] utilize retrieved tokens as input prompts and fine-tune the entire language model. Similar to the approach in [18], we employ retrieval samples as prompts to introduce pertinent information.

Recent advancements in CV also leverage external memory for various tasks. Several semi-parametric methods [21, 23, 28–30], including Tip-Adapter [21], have investigated the utilization of a k -nearest neighbor (kNN) classifier [31] to enhance classification performance without the need for fine-tuning. RAC [16] integrates the output of a *base* model, *i.e.*, a conventional vision encoder, with a retrieval module to address long-tail image classification challenges. Blattmann et al. [32] employ a semi-parametric diffusion model for generative image synthesis, which is augmented by a retrieval module.

Building upon the achievements of retrieval augmentation, we introduce a framework for few-shot classification and domain generalization through retrieval-based techniques. Our work focuses on retrieving examples from few-shot training data to construct more dynamic prompts for CLIP models. The most similar method to our own is *Training-free Adaption* (Tip-Adapter) [21]. Tip-Adapter solely employs retrieval to enhance the final classification distribution. We explore

the potential of using retrieval to improve the features extracted by CLIP models.

Finetuning for visual language models is crucial for bridging the domain gap in downstream tasks. While CLIP can perform zero-shot image classification by learning reasonable similarity in high-dimensional joint feature space between image-text pairs, finetuning with few-shot samples in a parameter-efficient manner remains meaningful. To achieve this, CoOP [6] substitutes the input context token in the text branch of CLIP with learnable parameters [33] for few-shot learning. Following recent advancements [34–36], we aim to optimize text prompts more effectively from a gradient perspective. CoCoOP [37] proposes to train an intermediate network to generate image tokens as conditional inputs for the text branch and design a base-to-new benchmark to evaluate the generalization ability of a method within a dataset. Some studies [8, 12–15] introduce trainable visual prompts [11] into the vision branch of CLIP to develop the dual prompt tuning scheme. Maple [13] proposes to learn layer-wise prompts for the two branches simultaneously. PromptSRC [15] utilizes its original features to regularize the learning of prompts.

Adapters are typically subnetworks consisting of two fully connected layers with a nonlinear activation function in between. Referring to the concept of adapters [38], CLIP-Adapter [7] employs lightweight adapters to adapt final features. Tip-Adapter [21] utilizes a key-value cache model for auxiliary classification. Sus-X [23] constructs a support set using generative models and extends Tip-Adapter by leveraging image-text affinity matrices. CaFO [30] improves visual recognition in low-shot regimes by expanding the training set through a generative model and integrating prior knowledge from multiple pre-training models using multiple adapters.

RePrompt provides an in-depth analysis of the key-value cache model from a retrieval perspective. It further explores the potential of this model to contribute to CLIP fine-tuning through retrieval-enhanced visual prompt learning. This approach enables RePrompt to effectively adjust the distribution of the image-feature space utilized in Tip-Adapter.

3 Preliminaries

CLIP [4] is a pre-trained model that learns aligned vision-language representations from web-scale image-text datasets. It comprises two sub-networks: an image encoder e_I and a text encoder e_T . The image encoder encodes visual inputs, and the text encoder encodes text inputs, into a shared hidden space \mathbb{R}^d . Here, d rep-

resents the dimension of embeddings (e.g., $d = 512$ for ViT [39] in CLIP).

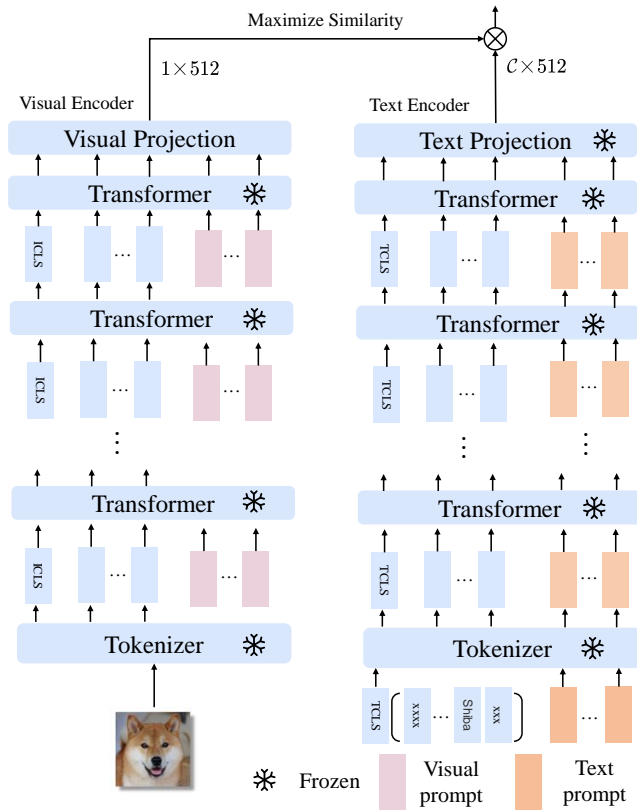


Fig. 1 The overall architecture of vision-language prompt tuning. Visual and textual prompt tokens, which are the only learnable parameters in this setup, are incorporated into the vision and language branches of CLIP, respectively. These prompts are designed to optimize performance in low-shot scenarios while preserving the model’s original generalization capabilities.

Classification of CLIP. Given an image \mathbf{x} and a set of C category names $T = \{t_1, t_2, \dots, t_C\}$ (e.g., $C = 1000$ for ImageNet [40]), the image encoder extracts the image feature $\mathbf{z} = e_1(\mathbf{x}) \in \mathbb{R}^d$. The category names in T are combined with a hand-crafted text prompt template “a photo of a [CLASS]” to generate text descriptions. These descriptions are then fed into the text encoder to derive the text features $\mathbf{f} \in \mathbb{R}^{d \times C}$. The prediction probability of \mathbf{x} belonging to class c is calculated using the inner product similarity between the query image feature \mathbf{z} and text features \mathbf{f} as shown in Equation 1:

$$p(c|x) = \frac{\exp((\mathbf{z} \cdot \mathbf{f}_c)/\tau)}{\sum_{c=1}^C \exp((\mathbf{z} \cdot \mathbf{f}_c)/\tau)}. \quad (1)$$

τ is the temperature coefficient learned by CLIP. The text encoder produces a retrieval-based dynamic classifier.

Text prompt learning. In contrast to hand-crafted prompt engineering, text prompt learning aims to generate more adaptive text features by learning a set of prompts. CoOp [6] learns a set of parameters $\mathbf{P}_T \in \mathbb{R}^{d \times M}$ to replace the predefined prompt templates, where M represents the prompt length. The word token of each category name in T is inserted into a template and treated as the initial values of learnable input prompts. These prompts are further fine-tuned on few-shot data to generate text features. The fine-tuned prompts \mathbf{P}_T adjust the decision boundaries of text features for downstream tasks. All parameters inherited from the pre-trained CLIP model remain fixed during the training process.

Visual prompt learning. VPT [11] proposes a visual prompt tuning approach, which introduces a few learnable parameters into the input space while freezing the image encoder e_1 . This method aims to extract more transferable visual features from downstream data. In the context of an image encoder with L layers, the output of the i -th layer, l_i , for $i = 1, 2, \dots, L$, can be expressed as:

$$[\mathbf{c}, \mathbf{z}_1^{i+1}, \dots, \mathbf{z}_S^{i+1}] = l_i(\mathbf{c}, \mathbf{z}_1^i, \dots, \mathbf{z}_S^i), \quad (2)$$

where $\mathbf{c} \in \mathbb{R}^d$ denotes the classification token and $\mathbf{Z}^i = \{\mathbf{z}_1^i, \dots, \mathbf{z}_S^i\} \in \mathbb{R}^{d \times S}$ represents a set of input image patch tokens of the i -th layer, with token sequence length S . Furthermore, the learnable visual prompt $\mathbf{P}_1 \in \mathbb{R}^{d \times N}$ is introduced into the input sequence of the i -th layer. N is the length of the visual prompt. There are two visual prompt variants, VPT-Shallow and VPT-Deep. In VPT-Shallow, the class token \mathbf{c} , along with image patch tokens and visual prompts, is taken as the input of the first layer. VPT-Deep inserts independent visual prompts into each layer.

In this section, we propose a straightforward baseline approach for few-shot image classification, named Vision-Language Prompt Tuning (VLPT). Figure 1 illustrates the overall architecture of VLPT. The visual prompt is optimized through visual prompt learning, while the text prompt is refined via text prompt learning. Upon deriving the image and text features for each category, the model with tuned prompts generates predictions based on the classification paradigm of clip.

4 Proposed Method

This section provides a detailed explanation of the proposed Retrieval-enhanced Prompt Tuning for VLPT. RePrompt enhances prompt tuning by utilizing the retrieval of relevant information from the training dataset. Given an input image x , RePrompt retrieves k potentially useful entries from the retrieval database. Each

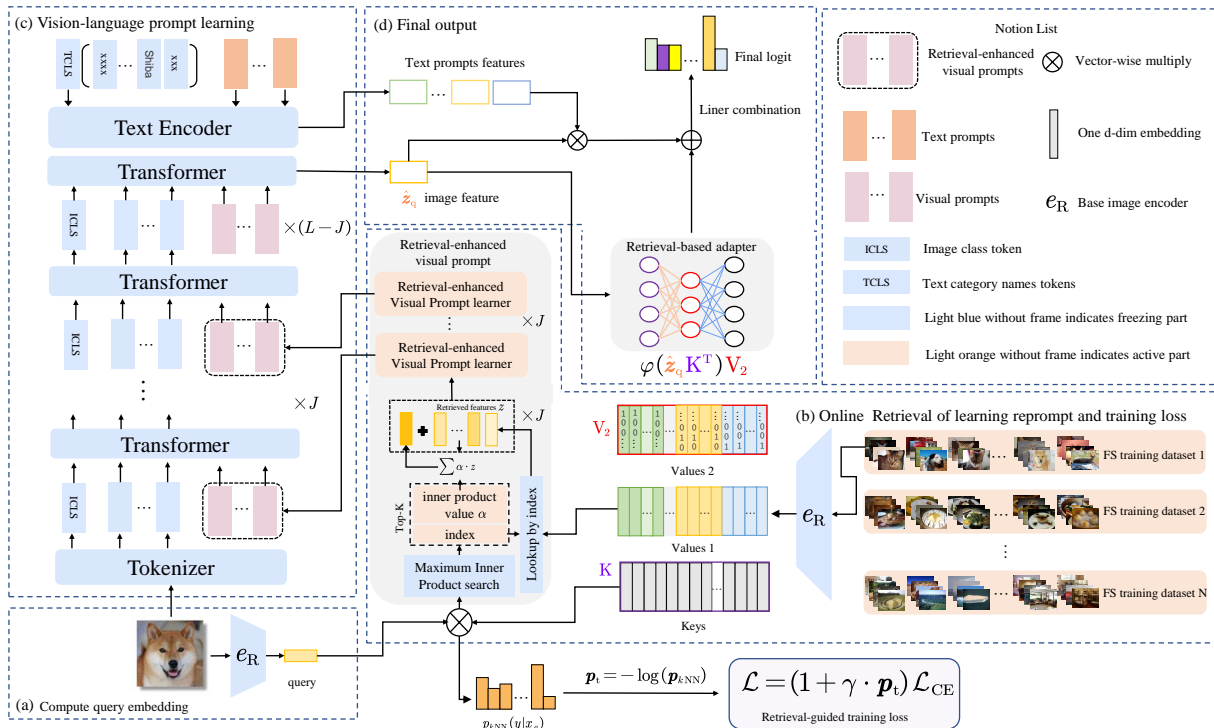


Fig. 2 The overall workflow of RePrompt includes four main steps: (a) Encoding an image input into a query embedding using a frozen image encoder; (b) Encoding each image entry from the training dataset into key and value embedding pairs with the same frozen image encoder, where the value embeddings also include one-hot representations of labels. We retrieve the top-K relevant knowledge items through maximum inner product search and integrate this knowledge to generate visual prompts; (c) Retrieval-enhanced visual prompts are introduced into the J layers of the visual branch inputs, while the other prompts remain consistent with those of the baseline VLPT; (d) The final output is derived from a linear combination of the prompt-tuned CLIP prediction and the retrieval-aided prediction.

entry is associated with a corresponding representation z and a label (the construction of the retrieval database is described in Section 4.1). The retriever uses embedding similarity to find relevant downstream knowledge in the retrieval database. We then condition on both the retrieved set and the original input x to generate the output through retrieval-enhanced visual prompt and retrieval-based adapter. Figure 2 illustrates the workflow of RePrompt. Specifically, Section 4.1 describes the process of retrieving entries most relevant to the input query. Subsequently, Section 4.2 details the prompt learner that integrates the query and retrieved knowledge into the prompt learning process. In Section 4.3, we discuss the final prediction in the inference process using the k NN-based probability from the retrieval-based adapter. Additionally, this section describes how non-parametric KNN is used between the query and the database to obtain probability distributions, while dynamically controlling the strength of the retrieval mechanism.

4.1 Retrieval module

Our Retrieval module consists of two steps: (1) building the database, and (2) retrieval.

Retrieval database. The retrieval database is constructed by extracting features from the few-shot training dataset \mathcal{D} . Specifically, the database contains $|\mathcal{D}|$ key-value pairs $(\mathbf{k}_i, \mathbf{v}_i)$. Each key $\mathbf{k}_i = \mathbf{e}_R(\mathbf{x}_i) \in \mathbb{R}^d$ represents the frozen training image representation extracted using \mathbf{e}_R . Each key-value pair comprises two components: the label $\mathbf{y} \in \mathbb{N}^+$ and the image representation $\mathbf{e}_R(\mathbf{x}_i) \in \mathbb{R}^d$. The retrieval database acts as a repository of robust tokens that are adaptable to changes in downstream tasks.

Previous studies [16, 17, 19] have demonstrated the effective performance improvements achieved by expanding the retrieval database. Direct use of external data can disrupt the few-shot task setting. To address this issue, we employ stable diffusion techniques [41] to generate additional training data for various categories. This approach allows us to expand the training data without requiring additional human effort for data collection and annotation. A straightforward template “a photo of a [CLASS]” is utilized as the text prompt. Subse-

quently, we employ CLIP to filter the top- \hat{K} images of the highest quality for each category. The selected images are added to the original retrieval database, expanding it with new samples and resulting in a total of $(K + \hat{K})$ training images across C categories. To ensure a fair comparison, synthesized data are not included in the training datasets used for the main experiments. In Table 5, we present the performance improvement achieved by incorporating synthesized data, demonstrating an average precision of 84.19% for the 16-shot scenario.

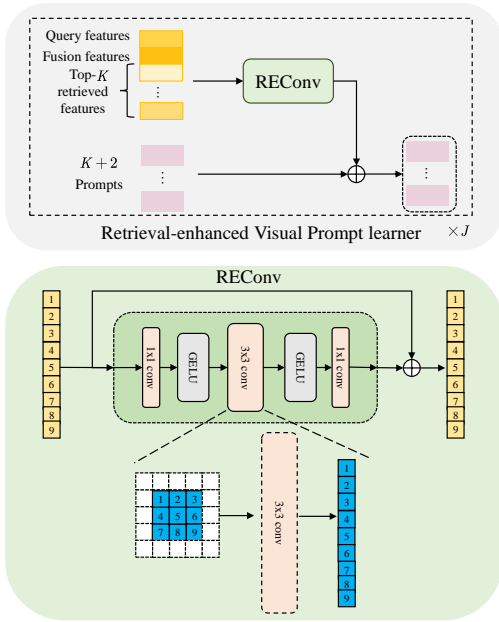


Fig. 3 Overview of visual prompt learner and REConv. A visual prompt learner comprises the REConv to generate dynamic visual prompts by learning on retrieved results

Effective and efficient retrieval. As shown in Figure 2, the retrieval database is represented as a matrix $D \in \mathbb{R}^{|\mathcal{D}| \times d}$, which serves as a fast approximate k -NN of examples. When presented with a query image x_q , we utilize the function e_R to map it to a corresponding vector $z_q = e_R(x_q)$. Using the query vector z_q , we retrieve its approximate k -nearest neighbors with representations z_1, z_2, \dots, z_k from the matrix D based on cosine similarity.

To demonstrate the impact of our retrieval mechanism and the influence of different e_R functions, we include visualizations of retrieved images corresponding to query samples in Figure 4. The visualization results demonstrate the retrieval’s capability to locate similar samples, with the image encoder of CLIP proving to be an effective e_R in identifying more accurately matched images. To ensure an efficient retrieval process, we employ FAISS [42] for querying the database.

4.2 Retrieval-enhanced visual prompt

The proposed method aims to enhance visual prompt learning by utilizing a retrieval database for analogy learning. The visual prompts generated from the retrieval results are referred to as retrieval-enhanced visual prompts.

The retrieval module receives a query vector z_q derived from a raw image x_q and performs a lookup operation in the matrix D to obtain the top k_{re} most similar candidates. The corresponding representations $z_1, z_2, \dots, z_{k_{re}}$ retrieved from the database are integrated into the image encoder to enhance the visual prompts. Additional fusion vectors $z_f \in \mathbb{R}^d$ [18] are generated by intuitively aggregating k_{re} neighboring representations based on their similarity, as follows:

$$z_f = \sum_{i=1}^{k_{re}} \alpha_i \cdot z_i, \quad \alpha_i = \frac{e^{z_q \cdot z_i}}{\sum_{j=1}^{k_{re}} e^{z_q \cdot z_j}}. \quad (3)$$

The query vectors z_q , fusion vectors z_f , and retrieved vectors $z_1, z_2, \dots, z_{k_{re}}$ are concatenated to form the input $\hat{i} = [z_q, z_f, z_1, \dots, z_{k_{re}}] \in \mathbb{R}^{d \times (k_{re}+2)}$ for the visual prompt learner, which then generates the retrieval-enhanced visual prompts $f_p(\hat{i}) \in \mathbb{R}^{d \times (k_{re}+2)}$.

As depicted at the top of Figure 3, we randomly initialize J visual prompt sets, P_1^1, \dots, P_1^J . Subsequently, J retrieval-enhanced convolution (REConv) blocks process J inputs, $\hat{i}_1, \dots, \hat{i}_J$ (by replicating \hat{i} J times), to generate dynamic prompts. These prompts are combined separately with the J visual prompt sets and inserted into the input sequences of the first J layers of the visual branch:

$$[c, Z^{j+1}] = l_j \left(c, f_p(\hat{i}_j) + P_1^j, Z^j \right), j = 1, \dots, J. \quad (4)$$

The remaining $12 - J$ layers process learnable prompts without enhancement, and learning these prompts reverts to conventional visual prompt tuning. Furthermore, we discuss the choice of insertion depth in subsection 6.2.

To effectively and efficiently fuse the retrieved representations, we propose a retrieval-enhanced convolution block (REConv). As illustrated at the bottom of Figure 3, a REConv block comprises three convolution layers: two 1×1 convolutions, which individually reduce and scale the channel dimensionality, and a 3×3 convolution positioned between the two 1×1 convolutions. Before these convolution layers, we reshape the 1D token sequence structure of visual prompts into a 2D matrix structure. REConv blocks process the input \hat{i} in parallel to generate dynamic prompts, which can be formulated as

$$f_p(\hat{i}_j) = \beta \text{REConv}_j(\text{LN}(\hat{i}_j)) + \hat{i}_j, \quad j = 1, \dots, J. \quad (5)$$

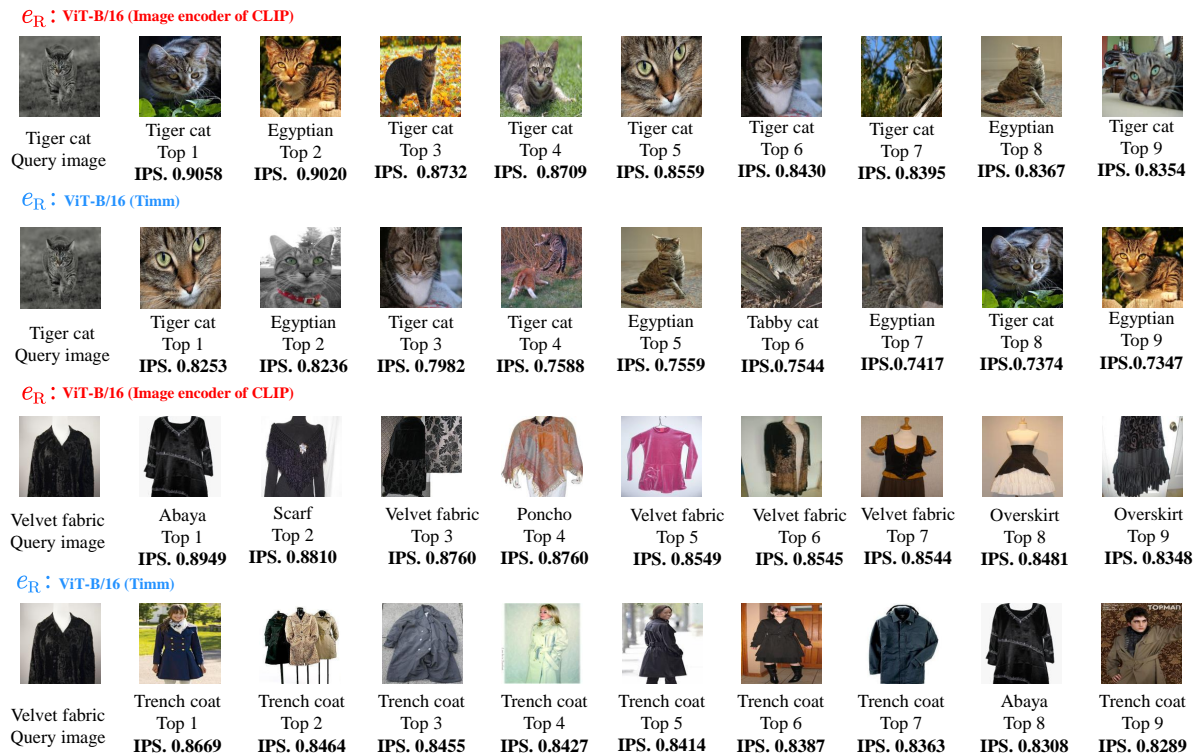


Fig. 4 Examples of the retrieval mechanism using various encoders e_R on ImageNet under the 16-shot setting. "ViT-B/16 (Image encoder of CLIP)" indicates that e_R utilizes the ViT-B/16 model as trained by CLIP. "ViT-B/16 (Timm)" denotes that e_R employs the ViT-B/16 model as trained by Timm with full supervision. "Top k " refers to the k nearest neighbors, and "IPS" represents the inner product similarity. Employing the image encoder of CLIP as e_R enhances the retrieval of visually similar and more accurate images, particularly for challenging samples such as "velvet fabric".

In this context, LN denotes Layer Normalization, and β is a hyper-parameter used for scaling the output.

4.3 Retrieval-based adapter

We regard Tip-Adapter as a retrieval-based adapter from the perspective of a k NN classifier framework. The adapter is trained in conjunction with the retrieval-enhanced visual prompt to enhance the generation of adaptive prediction probabilities for downstream tasks. The query vector, \hat{z}_q , is derived from a query instance, \mathbf{x}_q , using an image encoder that integrates retrieval-enhanced visual prompts. This vector retrieves the $|\mathcal{D}|$ nearest neighbors and their corresponding inner product similarities. We aggregate the probability mass for each label, \mathbf{y}_i , across all its occurrences among the retrieved targets. Assuming \mathbf{p}_{kNN} represents the probability of the query instance \mathbf{x}_q being classified as label \mathbf{y} , we then reformulate $\mathbf{p}_{kNN}(\mathbf{y} | \mathbf{x}_q)$ using a weighted sum of the \mathbf{p}_{kNN} probabilities as follows:

$$\mathbf{p}_{kNN}(\mathbf{y} | \mathbf{x}_q) \propto \sum_{(\mathbf{z}_i, \mathbf{y}_i) \in \mathcal{D}} \mathbf{1}_{\mathbf{y}=\mathbf{y}_i} \exp(\hat{z}_q \cdot \mathbf{z}_i). \quad (6)$$

To better integrate the prediction from the k NN and the base model, we interpolate $\mathbf{p}(\mathbf{y} | \mathbf{x}_q)$, blending the k NN prediction with the CLIP prediction, scaled by a factor λ :

$$\mathbf{p}(\mathbf{y} | \mathbf{x}_q) = \lambda \mathbf{p}_{kNN}(\mathbf{y} | \mathbf{x}_q) + (1 - \lambda) \mathbf{p}_P(\mathbf{y} | \mathbf{x}_q). \quad (7)$$

Relation to Tip-Adapter. Tip-Adapter constructs an adapter using a key-value cache model from the few-shot training set. The cache model stores prior knowledge encoded in CLIP and facilitates image classification through retrieval in the image embedding space. Tip-Adapter is considered as an auxiliary classifier that leverages image-image similarity. While both approaches aim to improve performance using retrieval, our paper highlights two key distinctions:

- (i) The features extracted by the CLIP image encoder with retrieval-enhanced prompts are more adaptive to downstream tasks compared to the features obtained by the original CLIP image encoder in Tip-Adapter. As a result, prompt-tuned query features can be utilized to compute improved image-image and image-text similarity matrices for classification.
- (ii) We extract potential visual context from the cache model and integrate it into the model in the form of

prompts, rather than considering the cache model solely as an adapter for classification assistance.

4.4 Retrieval-guiding training

The k -nearest neighbor (k NN) algorithm primarily focuses on approximating the neighborhoods of query instances [31]. It is intuitive to leverage k NN classification results as prior knowledge to guide RePrompt’s focus on hard examples during the training process. Hard samples usually refer to atypical samples with low confidence. To compute a local probability distribution, we limit the number of samples within the retrieved neighbor set $\mathbf{K} \subseteq \mathbf{D}$, where $k_{rc} \neq |\mathbf{K}|$, as follows:

$$\mathbf{p}_{k\text{NN}}(\mathbf{y} | \mathbf{x}_q) \propto \sum_{(\mathbf{z}_i, \mathbf{y}_i) \in \mathbf{K}} \mathbf{1}_{\mathbf{y}=\mathbf{y}_i} \exp(\mathbf{z}_q \cdot \mathbf{k}_i). \quad (8)$$

The probability $\mathbf{p}_{k\text{NN}}$ represents the confidence of classifying the query instance \mathbf{x}_q into specific categories. The negative log-likelihood value of $\mathbf{p}_{k\text{NN}}$, similar to Focal Loss [43], serves as the adjustment factor $\mathbf{p}_t = -\log(\mathbf{p}_{k\text{NN}})$. This adjustment factor modifies the relative loss of pseudo-correct or pseudo-error samples distinguished by k NN, thereby reweighting the cross-entropy loss \mathcal{L}_{CE} . The final loss is formulated as follows:

$$\mathcal{L} = (1 + \gamma \cdot \mathbf{p}_t) \mathcal{L}_{\text{CE}}, \quad (9)$$

where γ is a scaling factor. We set $|\mathbf{K}| = C \times n$, $n \in \mathbb{N}^+$ [18], which adopts a similar loss for augmenting the model performance on the few-shot learning task of NLP. In few-shot experiments, n can take values of 1, 2, 4, 8, 16 to accommodate different few-shot settings. We discuss the choice of n in Table 10.

5 Experiments

5.1 Few-shot classification

Datasets. The RePrompt model is evaluated on 11 image classification datasets, covering various tasks such as object recognition (ImageNet1k [40] and Caltech101 [44]), fine-grained object recognition (Oxford Pets [45], Flowers102 [46], FGVC Aircraft [47], Stanford Cars [48], and Food101 [49]), sense recognition (SUN397 [50]), remote sensing recognition (EuroSAT [51]), texture recognition (DTD [52]), and action recognition (UCF101 [53]). we construct 1,2,4,8,16-shot training sets with full categories and the entire test set.

Baseline. We compare our proposed RePrompt with these existing prompt-based approaches: CoOP [6], VPT-Deep [11], Maple [13], PromptSRC [15], Tip-Adapter [21],

Tip-Adapter-F [21], and VLPT. (1) CoOP learns the context prompt concatenated with [CLASS] as the input of text encoder. (2) VPT-Deep incorporates learnable visual prompts into each transformer layer of the visual encoder. (3) VLPT jointly optimizes prompts across different modality encoders, following the methodologies of CoOP and VPT-Deep. (4) Tip-Adapter constructs a cache-model-based adapter using few-shot training data. It is a model which performs few-shot predictions by using those retrieved samples in the end, simply by making some prototypes. (5) Tip-Adapter-F is the variant where the adapter is fine-tuned. (6) Maple learns prompts for the text and image branches simultaneously, rather than a separate side. (7) PromptSRC uses the clip’s original features to regularize the prompt learning.

Training details. Prompt tuning, originally introduced in NLP, is extended to unified visual and language models by implementing it on a ViT model, specifically ViT-B/16, with 12 transformer layers similar to the text encoder. The hyper-parameters of the retrieval modules are set as follows: k_{re} is set to 7, and 9 random prompts are initialized. The first 7 layers of the vision transformer are equipped with retrieval-enhanced prompts. The prompt and adapter are fine-tuned using the AdamW optimizer with a learning rate of 1e-3 and an epsilon value of 1e-4. We adhere to the data preprocessing protocol of CoOP [6] and freeze the parameters inherited from the pre-trained model during training.

Results. The performance of baseline approaches and our proposed RePrompt for few-shot image classification is presented in Figure 5. In general, parameter-efficient finetuning methods perform better than zero-shot classification (zero-shot CLIP) in scenarios with an average of over 11 datasets. RePrompt overall provides consistent improvements on most shots in comparison with all existing methods. RePrompt demonstrates significant performance improvement, particularly with +5.87% accuracy on DTD and +9.04% accuracy on Stanford Cars, based on VLPT. RePrompt substantially enhances performance on challenging datasets that contain a wide range of categories, such as ImageNet with 1000 classes and SUN397 with 397 classes. We also observe that RePrompt achieves fewer improvements on Oxford Pets and Food101. This could be attributed to the presence of noisy data and unique data distribution patterns in these datasets [6, 12, 49].

5.2 Cross-dataset evaluation

We evaluate the cross-dataset generalization ability of RePrompt by learning on the 16-shot ImageNet setting and then transferring it directly to the remaining 10

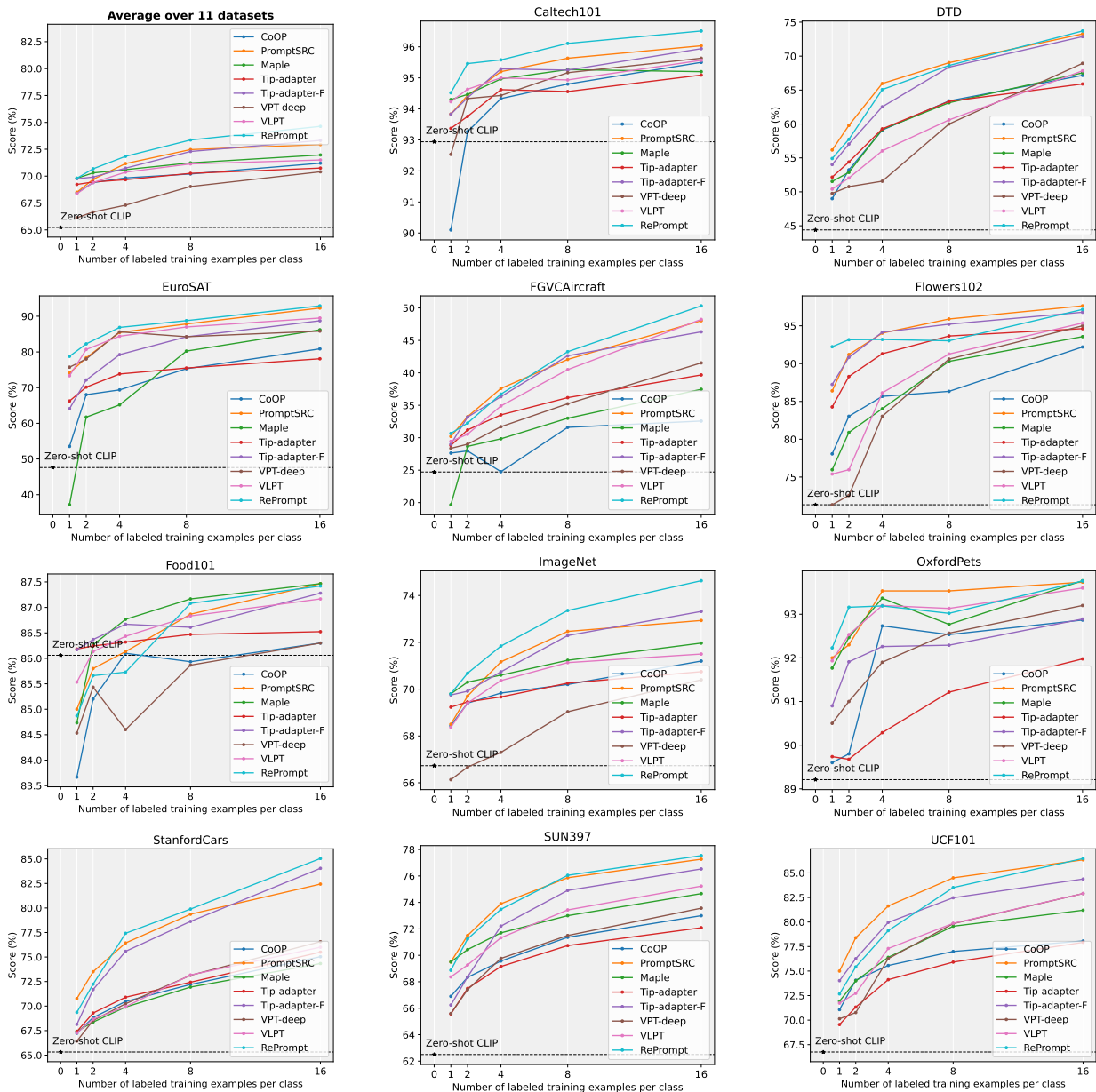


Fig. 5 Main results over 11 datasets under the few-shot settings. We report the average accuracy(%) of three runs for 1,2,4,8,16 shots. The proposed RePrompt achieves significant performance improvements on most downstream recognition datasets.

datasets. Since this evaluation does not provide training images for other datasets, we remove the retrieval-based adapter module from this test. Table 3 shows the performance comparison between CoOP, CoCoOP, Maple, and PromptSRC. On the ImageNet source dataset, RePrompt achieves the best performance and demonstrates a strong generalization performance by surpassing recent SOTA methods in 5 datasets.

5.3 Domain generalization

Pre-trained vision-language models exhibit a robust ability for domain generalization ability [6]. We assess the robustness of the proposed RePrompt model on out-of-distribution (OOD) datasets.

Datasets. We follow CoOp [6] and employ five datasets, namely, ImageNet, ImageNet V2 [54], ImageNet-Sketch [55], ImageNet-A [56] and ImageNet-R [57]), to evaluate the generalization ability of RePrompt for out-of-distribution (OOD) data. Following the protocol, we train the model on the ImageNet dataset (as the source

| Methods | ImagNet | V2 [54] | S [55] | A [56] | R [57] |
|----------------|--------------|--------------|--------------|--------------|--------------|
| CoOP [6] | 71.51 | 64.20 | 47.99 | 49.71 | 75.21 |
| CoCoOP [37] | 71.02 | 64.07 | 48.75 | 50.63 | 76.18 |
| UPT [12] | 72.63 | 64.35 | 48.66 | 50.66 | 76.24 |
| Maple [13] | 70.72 | 64.07 | 49.15 | 50.90 | 76.98 |
| PromptSRC [15] | 71.27 | 64.07 | 49.55 | 50.90 | 77.80 |
| RePrompt | 74.53 | 66.66 | 49.56 | 49.77 | 77.48 |

Table 1 Main results under the domain generalization setting. We report the average accuracy (%) of 16 shots over three runs.

| Model | MVIImgNet | | | | | |
|------------------|-------------|-------------|-------------|-------------|-------------|-------------|
| | 1-shot | 2-shot | 4-shot | 8-shot | 16-shot | Ave. |
| Vanilla CLIP [4] | 51.4 | 51.4 | 51.4 | 51.4 | 51.4 | 51.4 |
| CoOP* [6] | 62.5 | 67.8 | 75.3 | 79.8 | 84.0 | 73.9 |
| VLPT | 65.2 | 69.7 | 76.8 | 80.3 | 84.9 | 75.3 |
| RePrompt | 65.9 | 73.6 | 81.1 | 85.7 | 90.8 | 79.4 |

Table 2 Main results on MVIImgNet under the few-shot multi-view settings. RePrompt achieved significant performance improvements due to its retrieval-enhanced module.

dataset) using a 16-shot setting and evaluate its performance on other domain-shifted datasets (as the target datasets). Consequently, we utilize the retrieval database from the ImageNet 16-shot experiment as the retrieval database for the target datasets.

Results. Table 1 summarizes the OOD experiment results, including the accuracy on both source datasets and target datasets. RePrompt achieves optimal results on ImageNet V2 and ImageNet-Sketch while demonstrating performance comparable to PromptSRC [15] on ImageNet-R. These results indicate that RePrompt has better generalization for datasets with domain shifts.

5.4 Other few-shot classification

We investigate the ability of RePrompt to bridge the modality gap in video and multi-view domains.

Datasets. MVIImgNet [62] is a 3D generic dataset that comprises multi-view images, which is a soft bridge between 2D and 3D. It contains 6.5 million frames from 219188 videos, accompanied by comprehensive annotations. These frames covers real-life objects across from 238 classes. Nevertheless, MVIImgNet displays a long-tailed distribution of data. Consequently, we eliminate categories with fewer than 16 samples and samples with fewer than 28 frames. In the end, we obtained a subset of MVIImgNet, consisting of a total of 220 classes. We adopt the same few-shot setting as used in few-shot image classification. The video understanding task covers HMDB-51 [63], UCF-101 [53] and SSV2 [64], where each dataset consists of 2/4/8/16-shot training sets with full categories. The model are evaluated on the first validation split for HMDB-51, UCF-101, and the whole validation split for SSV2.

Training details. We adopt a sparse frame-sampling strategy [65] and configure the number of frames as

16 for multi-view classification and 32 for video understanding. For the video understanding task, models are pre-trained on Kinetics-400 [66] to bridge the modality gap and follow a single-view inference [61]. The retrieval setup aligns with that of few-shot image classification. However, the training hyperparameters remain consistent with those of ViFi-CLIP-Prompting [61]. The minimum retrieval unit in the database is a frame-level embedding, aligned with the input data. The weights of the “Rb adapter” are sourced from another database, where the minimum retrieval unit is a video-level embedding. The use of pooling for simple frame-level temporal aggregation enables the exchange of temporal and multi-view cues in CLIP representations.

Results. Table 2 demonstrates the RePrompt consistently improves performance as the number of shots increases in multi-view classification. For example, it achieves a gain of +4.2% compared to VLPT. This improvement can be attributed to the retrieval process, which brings more reference information from different perspectives. Table 4 illustrates the effectiveness of RePrompt compared to other CLIP-based approaches for videos. Notably, RePrompt achieves larger gains in low-shot data scenarios, where models are more susceptible to overfitting.

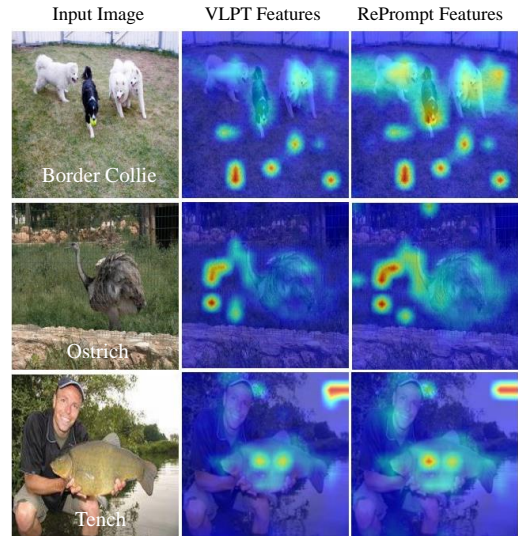


Fig. 6 Visualization of attention response map between retrieval-enhanced visual prompts and image patch tokens. The mean self-attention map is from the last vision transformer layers.

5.5 Ablation

Component ablation. We investigate the effectiveness of RePrompt and report results in Table 5. A progressive approach of incorporating retrieval modules

| Method | Source | | | | | Target | | | | | | | Avg. |
|----------------|--------------|--------------|--------------|---------------|--------------|--------------|---------------|--------------|--------------|--------------|--------------|--------------|------|
| | ImageNet | Caltech 101 | Oxford Pets | Stanford Cars | Flowers 102 | Food101 | FGVC Aircraft | SUN397 | DTD | Euro SAT | UCF101 | | |
| CoOP [6] | <u>71.51</u> | 93.70 | 89.14 | 64.51 | 68.71 | 85.30 | 18.47 | 64.15 | 41.92 | <u>46.39</u> | 66.55 | 63.88 | |
| CoCoOP [37] | 71.02 | <u>94.43</u> | 90.14 | 65.32 | 71.88 | 86.06 | 22.94 | <u>67.36</u> | 45.73 | 45.37 | 68.21 | 65.74 | |
| Maple [13] | 70.72 | 93.53 | 90.49 | 65.57 | <u>72.23</u> | 86.20 | 24.74 | 67.01 | <u>46.49</u> | 48.06 | 68.69 | 66.30 | |
| PromptSRC [15] | 71.27 | 93.60 | <u>90.25</u> | <u>65.70</u> | 70.25 | <u>86.15</u> | 23.90 | 67.10 | 46.87 | 45.50 | <u>68.75</u> | 65.81 | |
| RePrompt | 74.53 | 94.65 | 90.16 | 67.76 | 72.47 | 86.00 | <u>24.33</u> | 67.71 | 44.39 | 41.74 | 69.28 | <u>65.85</u> | |

Table 3 Comparison of RePrompt with existing advanced approaches on cross-dataset benchmark evaluation. The source model (ViT-B/16) is trained on ImageNet [40]. RePrompt achieves the best results on 5 of 10 datasets. The underline represents the second best.

| Model | HMDB-51 | | | | | UCF-101 | | | | | SSV2 | | | | |
|------------------|-------------|-------------|-------------|-------------|-------------|-------------|-------------|-------------|-------------|-------------|------------|------------|-------------|-------------|------------|
| | 2-shot | 4-shot | 8-shot | 16-shot | Ave. | 2-shot | 4-shot | 8-shot | 16-shot | Ave. | 2-shot | 4-shot | 8-shot | 16-shot | Ave. |
| Vanilla CLIP [4] | 41.9 | 41.9 | 41.9 | 41.9 | 41.9 | 63.6 | 63.6 | 63.6 | 63.6 | 63.6 | 2.7 | 2.7 | 2.7 | 2.7 | 2.7 |
| ActionCLIP [58] | 54.3 | 56.2 | 59.3 | 66.1 | 59.0 | 76.7 | 80.4 | 87.6 | 91.8 | 84.1 | 4.8 | 6.9 | 9.1 | 12.3 | 8.3 |
| XCLIP [59] | 60.5 | 66.8 | 69.3 | 71.7 | 67.1 | 89.0 | 91.4 | 94.7 | 96.3 | 92.9 | 6.6 | 7.8 | <u>9.9</u> | <u>13.7</u> | 9.5 |
| A5 [60] | 46.7 | 50.4 | 61.3 | 65.8 | 56.1 | 76.3 | 84.4 | 90.7 | 93.0 | 86.1 | 4.5 | 6.7 | 7.2 | 9.5 | 7.0 |
| ViFi-CLIP* [61] | 61.3 | 65.3 | 68.1 | 70.1 | 66.4 | <u>90.4</u> | <u>92.9</u> | <u>94.4</u> | 95.7 | 93.3 | 7.2 | 8.1 | 10.2 | 13.9 | 9.7 |
| RePrompt | 63.4 | 67.6 | 69.2 | 71.1 | 67.8 | 91.2 | 93.5 | 95.0 | <u>95.4</u> | 93.7 | 7.6 | 9.3 | 9.4 | 12.1 | <u>9.6</u> |

Table 4 We compare RePrompt with approaches that explicitly adapt CLIP. ViFi-CLIP only adds an average pooling layer on top of the final features to obtain video-level embeddings. The underline represents the second best.

| Method | EuroSAT | Caltech101 | Flowers102 | Food101 | FGVCAircraft | DTD | OxfordPets | StanfordCars | UCF101 | SUN397 | ImageNet | average |
|---------------------|--------------|--------------|--------------|--------------|--------------|--------------|--------------|--------------|--------------|--------------|--------------|--------------|
| CoOP* [6] | 80.87 | 95.50 | 92.20 | 86.30 | 32.57 | 67.17 | 92.87 | 75.03 | 78.07 | 73.00 | 71.20 | 76.80 |
| VPT-deep* [11] | 85.83 | 95.63 | 95.00 | 86.30 | 41.53 | 68.93 | 93.20 | 76.57 | 82.90 | 73.57 | 70.40 | 79.80 |
| PromptSRC* | 92.30 | 96.03 | 97.63 | 87.47 | 48.03 | 73.27 | 93.73 | 82.43 | 86.33 | 77.27 | 72.93 | 82.49 |
| Maple* [13] | 86.20 | 95.20 | 93.57 | 87.47 | 37.47 | 67.53 | 93.77 | 74.33 | 81.20 | 74.67 | 71.97 | 78.49 |
| Tip-Adapter [21] | 78.09 | 95.09 | 94.62 | 86.52 | 39.68 | 65.90 | 91.98 | 75.50 | 77.93 | 72.09 | 70.75 | 77.10 |
| Tip-Adapter-F* [21] | 88.74 | 95.94 | 96.79 | 87.28 | 46.32 | 72.87 | 92.89 | 84.04 | 84.38 | 76.53 | 73.32 | 81.74 |
| +VLPT | 89.50 | 95.57 | 95.37 | 87.17 | 48.04 | 67.83 | 93.60 | 76.00 | 82.90 | 74.20 | 71.42 | 80.14 |
| +Rg training loss | 92.48 | 96.55 | 94.72 | 87.56 | 47.94 | 69.74 | 93.54 | 74.18 | 83.53 | 75.20 | 72.00 | 80.68 |
| +Re visual prompt | 92.60 | 96.55 | 96.79 | 87.57 | 48.27 | 70.63 | 93.62 | 77.85 | 83.95 | 75.60 | 72.20 | 81.42 |
| +Rb adapter | 92.91 | 96.51 | 97.16 | 87.42 | 50.32 | 73.70 | 93.76 | 85.04 | 86.47 | 77.54 | 74.53 | 83.21 |
| CaFO-F* [30] | 91.72 | 97.28 | 97.97 | 87.15 | 54.82 | 71.34 | 93.89 | 83.85 | 86.10 | 76.62 | 74.48 | 83.20 |
| Reprompt+synt. data | 91.95 | 96.80 | 98.29 | 87.23 | 55.21 | 76.18 | 93.92 | 87.55 | 87.34 | 77.39 | 74.23 | 84.19 |

Table 5 Component ablation studies over 11 datasets with 16-shot setting. The average accuracy of RePrompt has been steadily improved through the gradual introduction of retrieval enhancement modules.

is employed to demonstrate the efficacy of enhancement measures at various stages. The average accuracy of RePrompt consistently improves as we incrementally introduce retrieval augmentation: Retrieval-guiding training denoted as +Rg training loss, Retrieval-enhanced visual prompt denoted as +Re visual prompt, and Retrieval-based adapter denoted as +Rb adapter. We also evaluated the Tip-adapter, which solely utilizes the retrieved samples as prototypes. The findings indicate that retrieval-enhanced visual prompts significantly enhance retrieval-based classification results.

Furthermore, we visualize the attention map in the last layer of the image encoder for both VLPT and RePrompt to illustrate the impact of retrieval-enhanced visual prompts. The visualization results, displayed in Figure 6, reveal that RePrompt has more pronounced self-attention responses, characterized by expanded areas of interest and heightened attention values. This en-

hancement correlates with a performance improvement of "+1.28%", attributable to the inclusion of "+Re visual prompt".

The noticeable improvement achieved with the "+Rb adapter" can be ascribed to its capability to introduce additional degrees of freedom for the query features, which is unattainable with the conventional Tip-Adapter-F. Tip-Adapter operates as a training-free approach, leveraging the similarity of image features to aid in classification. Despite attempts to mitigate this limitation through fine-tuning in Tip-Adapter-F, the query features remain unchanged. The limited ability of Tip-Adapter-F to manipulate query features significantly hampers its performance.

To further substantiate these observations, we employ t-SNE [67] to visualize the 3D manifold of test features extracted from the CLIP, VLPT, and RePrompt models on the EuroSAT dataset. The t-SNE visual-

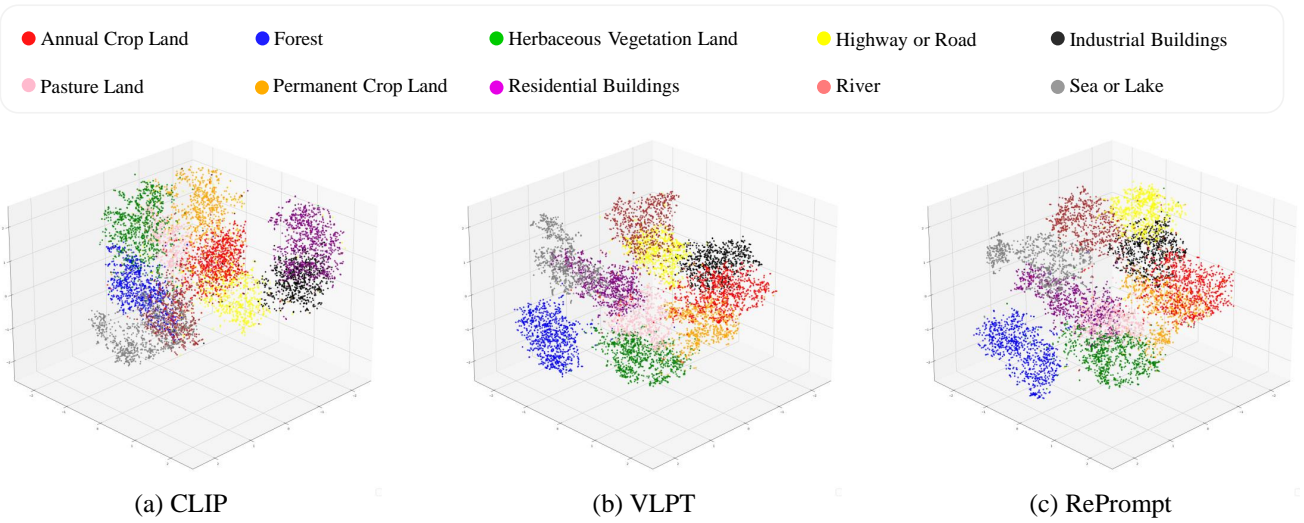


Fig. 7 Visualization of different learned visual feature manifolds via t-SNE. From left to right, we have CLIP, VLPT, and RePrompt. The image features extracted by RePrompt are more discriminating along the z-axis.

ization results, presented in Figure 7, clearly depict that in the high-dimensional classification space, RePrompt achieves a much more distinct separation of image features, with feature distributions more aligned along the z-axis, distinguishing between various categories. Conversely, Tip-Adapter-F, constrained by a frozen visual encoder, exhibits t-SNE visualization results that closely resemble those of CLIP, with considerable overlap in feature distribution. This overlap elucidates why Tip-Adapter performs suboptimally on remote sensing data such as EuroSAT.

Expanding retrieval database. We follow recent approaches [23,30] that leverage a powerful text-to-image generative model, Stable Diffusion [41], to construct a pseudo training set or expanding the existing training set. The K is set to 2. In the bottom row of Table 5, our results demonstrate that RePrompt benefits from synthesis data and achieves state-of-the-art performance (average accuracy 84.19%). Compared to CaFO [30], an improvement method of Tip-Adapter-F, RePrompt achieves an average precision improvement of +0.99 %.

Discussions on ReConv and retrieved samples. We explore the impact of the network structure, which is responsible for integrating tokens and queries, on the performance outcomes of the ReConv model. To this end, we conduct a supplementary experiment on ImageNet, where we substitute the convolution layer in ReConv with different layers. ReRNN is a variant in which the convolution layer is replaced with an LSTM layer [68, 69]. ReMLP replaces the convolution layer with a multi-layer perceptron layer. Additionally, the quality of high-retrieval samples also contributes to performance; hence, we examine the effect of utilizing original features and random sample features as inputs.

| method | 16-shot | 8-shot | 4-shot | 2-shot | 1-shot |
|-----------------|--------------|--------------|--------------|--------------|--------------|
| ReMLP | 74.21 | 73.02 | 71.40 | 70.33 | 69.50 |
| ReRNN | 74.27 | 72.60 | 71.12 | 70.32 | 69.49 |
| ReConv(z_q) | 74.34 | 72.51 | 70.84 | 70.42 | 69.33 |
| ReConv+Random | 74.03 | 72.43 | 70.68 | 69.98 | 66.96 |
| ReConv | 74.53 | 73.36 | 71.84 | 70.68 | 69.87 |

Table 6 Ablation study of the visual prompt learner across different input strategies and network structures. The first two rows showcase results using RNN and MLP structures, respectively. The middle two rows illustrate the impact of using original image features and random sample features as inputs. ReConv consistently outperforms the other variations, demonstrating its effectiveness across varying shot scenarios.

ReConv(z_q) is a variant that exclusively uses z_q as input, whereas ReConv+Random employs random sample features. The experimental setup for these variants aligns with that of ReConv, maintaining a comparable number of parameters across both models.

As demonstrated in Table 6, ReConv marginally outperforms the other variants across all shot levels. These results suggest that the specific network structure used for token and query fusion may not significantly affect the overall model performance. Instead, the choice of network structure should take into account the computational cost and optimization challenges, particularly as task complexity increases. However, the quality of retrieval samples plays a crucial role, implying that expanding the search library and enhancing the search methodologies are of greater importance.

Training and inference compute cost analysis. The compute cost and efficiency analysis is listed in Table 7 and Table 8 for 16-shot classification on ImageNet. “Wo Retrieval” is a comparative model with the same number of learnable parameters as RePrompt. RePrompt shows a promising balance between accuracy and inference efficiency, achieving 74.53% accuracy with

| Methods | Acc.(%) | Param.(M) | Train. | Epochs |
|--------------------|---------|-----------|----------|--------|
| CoOP [6] | 71.20 | 0.4 | 14h40min | 200 |
| Tip-Adapter-F [21] | 73.32 | 8.19 | 5min | 20 |
| VLPT | 71.42 | 0.45 | 15h50min | 100 |
| Wo Retrieval | 71.91 | 11.11 | 3h30min | 20 |
| RePrompt | 74.53 | 11.11 | 4h | 20 |

Table 7 Comparison of training efficiency for different methods on 16-shot ImageNet. All experiments are trained with batch 16 on one RTX309 GPU.

| Methods | Acc.(%) | Inference time (ms) | GFLOPs(inference) |
|--------------------|---------|---------------------|-------------------|
| CoOP [6] | 71.20 | 299.64 | 162.5 |
| Tip-Adapter-F [21] | 73.32 | 10.5 | 42.5 |
| VLPT | 71.42 | 214.84 | 162.5 |
| Wo Retrieval | 71.91 | 17.57 | 76.5 |
| RePrompt | 74.53 | 57.60 | 76.5 |

Table 8 Comparison of inference efficiency for different methods on 16-shot ImageNet. All experiments are trained with batch 16 and tested with batch size 32 on one RTX309 GPU.

relatively low inference time (57.60 ms) and moderate computational demand (76.5 GFLOPs). Furthermore, we reduce the training time to only 20 epochs, in contrast to CoOP. **In comparison to Tip-Adapter-F, RePrompt provides undeniable performance advantages and superior cross-domain adaptability.** Additionally, the retrieval time during inference is about 40 ms, which is deemed acceptable for few-shot image classification.

Overall, these results highlight the trade-offs between training duration, model complexity, computational efficiency, and performance, emphasizing the effectiveness of RePrompt in leveraging retrieval for improved few-shot classification on high-complexity tasks.

6 Retrieval Discussions

Given that the retrieval database is constructed from training data in a few-shot setting, the performance enhancements observed with RePrompt are intimately linked to data statistics. To delve deeper, we investigate the correlation between the efficacy of retrieval enhancement and the intra-class variance of visual features. This specific relationship is depicted in Figure 8, illustrating the association between intra-class visual variance and performance improvement. Aside from the outliers—“StanfordCars” and “DTD”—the remaining datasets exhibit a discernible pattern. Notably, the labels for StanfordCars correspond to vehicle codes, and those for DTD to texture descriptions, categories where CLIP’s classification capabilities manifest notable deficiencies. Consequently, results from these two datasets are excluded from the general analysis to delineate retrieval enhancement patterns more accurately.

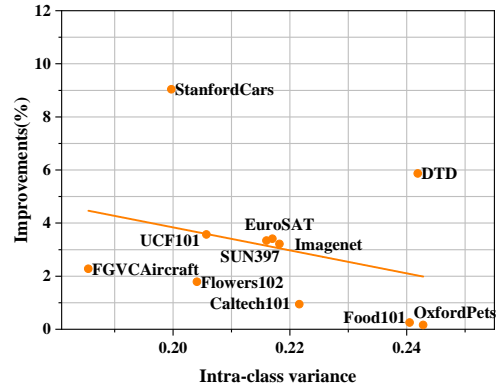


Fig. 8 Visualization of the Correlation Between Performance Improvements and Intra-class Visual Variance. The graph demonstrates a general trend where the performance improvements offered by RePrompt tend to decrease as the intra-class visual variance increases. This suggests a sensitivity of the RePrompt’s efficacy to the homogeneity of visual features within classes.

6.1 Analysis of retrieval

Experiments are conducted across FGVC Aircraft, Oxford Pets and ImageNet-1K to quantitatively assess the influence of retrieval in various few-shot scenarios. FGVC Aircraft has the smallest intra-class visual variance, while Oxford Pets has the largest; ImageNet-1K falls intermediate between these two. By comparing the optimal retrieval parameter adjustments among these datasets, we can analysis the influence of intra-class visual variance on the retrieval mechanism.

The increasing value of the **retrieval-enhanced prompt number** $k_{re} + 2$ indicates that RePrompt benefits from additional retrieved information. As illustrated in Table 9, the optimal k_{re} parameter varies among the three datasets. Specifically, we observe that $k_{re} = 14$ consistently underperforms across all few-shot settings for Oxford Pets. This suggests that the retrieved information is detrimental and lacks confidence in contexts with significant intra-class visual variance. In contrast, $k_{re} = 14$ demonstrates improved average performance on FGVC Aircraft, underscoring its utility in scenarios with lesser intra-class variance.

The factor n determines **the number of retrieval samples**, $|\mathbf{K}| = C \times n$, used in retrieval-guiding training loss. Increasing the value of n signifies a more relaxed constraint on retrieval. As shown in Table 10, $n = 1$ achieves optimal performance in the 16-shot setting on Oxford Pets, which implies that RePrompt prefers the output of CLIP with retrieval-enhanced prompt. However, in low-shot scenarios (e.g., $n = 2/1$ under $2/1$ -

| $k_{re}+2$ | Dataset | 16-shot | 8-shot | 4-shot | 2-shot | 1-shot | Ave |
|------------|---------------|--------------|--------------|--------------|--------------|--------------|---------------|
| 2+2 | FGVC Aircraft | 53.05 | 45.84 | 39.39 | 34.86 | 31.05 | 40.838 |
| 7+2 | | 54.61 | 47.94 | 40.05 | 35.61 | 31.23 | 41.888 |
| 14+2 | | 54.91 | 47.97 | 40.17 | 35.79 | 31.17 | 42.002 |
| 2+2 | Oxford Pets | 94.58 | 93.84 | 93.21 | 92.97 | 91.55 | 93.23 |
| 7+2 | | 94.85 | 93.57 | 93.62 | 92.94 | 91.82 | 93.36 |
| 14+2 | | 94.47 | 93.65 | 93.16 | 93.21 | 91.41 | 93.18 |
| 2+2 | ImageNet | 74.50 | 73.23 | 71.51 | 70.53 | 69.46 | 71.85 |
| 7+2 | | 74.53 | 73.28 | 71.38 | 70.40 | 69.87 | 71.89 |
| 14+2 | | 74.40 | 73.11 | 71.29 | 70.35 | 69.64 | 71.76 |

Table 9 Ablation study on different visual prompt numbers over Fgvc Aircraft and Oxford Pets with few-shot settings. The retrieval-enhanced prompt is mainly affected by the convolution kernel size of REConv.

shot setting), RePrompt may require more additional references due to the scarcity of training data.

| n | Dataset | 16-shot | 8-shot | 4-shot | 2-shot | 1-shot |
|-----|---------------|--------------|--------------|--------------|--------------|--------------|
| 16 | FGVC Aircraft | 54.40 | — | — | — | — |
| 8 | | 54.61 | 47.94 | — | — | — |
| 4 | | 54.79 | 47.28 | 40.11 | — | — |
| 2 | | 54.04 | 47.31 | 39.96 | 35.81 | — |
| 1 | | 54.58 | 47.31 | 40.05 | 35.43 | 31.23 |
| 16 | Oxford Pets | 94.60 | — | — | — | — |
| 8 | | 94.49 | 93.43 | — | — | — |
| 4 | | 94.55 | 93.57 | 93.62 | — | — |
| 2 | | 94.69 | 93.51 | 93.21 | 92.94 | — |
| 1 | | 94.85 | 93.46 | 93.57 | 92.70 | 91.82 |
| 16 | ImageNet-1k | 74.30 | — | — | — | — |
| 8 | | 74.53 | 73.11 | — | — | — |
| 4 | | 74.26 | 73.30 | 71.52 | — | — |
| 2 | | 74.31 | 73.16 | 71.50 | 70.40 | — |
| 1 | | 74.37 | 73.23 | 71.24 | 70.38 | 70.02 |

Table 10 Ablation studies on retrieving n samples for each class over Fgvc Aircraft and Oxford Pets with few-shot settings. The k NN-guiding training is weak in low-shot settings, since the model may require reference on the k -nn classifier.

Based on the above analysis, we summarize two empirical rules as follows: 1) For a dataset with low or high intra-class visual variance, it is imperative to employ a retrieval model with correspondingly strong or weak capabilities to guarantee stable performance improvements across scenarios. 2) In low-shot settings, the inference outcomes are dominantly influenced by the retrieval results.

6.2 Tuning retrieval parameters

The final prediction distribution in RePrompt is influenced by the hyperparameters γ and λ , and the prompt depth J . Ablation experiments are conducted to investigate the impact of these hyperparameters on the final outcomes across different datasets.

As illustrated in Figure 9, from top to bottom, ablation experiments are carried out on FGVC Aircraft, ImageNet, and Oxford Pets under the 16-shot learning setting. The experiments adhere to the default configurations, except for modifying the depth J , γ , and λ parameters. The experiment data are averaged over the results of experiments on seeds 1,2,3. The reference configuration is marked by a gray vertical dotted line.

λ varies. The hyper-parameter λ controls the degree of combination between adapter predictions, acting as a weight factor for the prompt-tuned CLIP and the k -NN classifier. A higher λ value signifies an increased reliance on knowledge from the retrieval module. As depicted in the left segment of Figure 9, it is evident that the performance demonstrates overall improvement as λ increases from 0.0 to 0.5. Notably, this progression yields the highest accuracy: 54.67% for FGVC Aircraft ($\lambda = 0.8$), 74.59% for ImageNet ($\lambda = 0.4$), and 94.5% for Oxford Pets ($\lambda = 0.5$). Post the peaks, a decline in accuracy is observed as λ increases beyond the optimal points. This trend suggests that while an increase in λ generally benefits the integration of retrieval-based knowledge, excessive weighting can lead to a reliance on potentially noisy or less relevant retrieved information.

J varies. Depth J denotes the insertion depth of the retrieval-enhanced prompt. From the medium part of Figure 9, we find that a moderate insertion depth of retrieval-enhanced prompt is optimal, 54.86% at the first 2 layers for FGVC Aircraft, 74.52% at the first 7 layers for ImageNet, and 94.37% at the first 6 layers for Oxford Pets. The graph further reveals fluctuating performance across different layer depths, indicating that not all layers equally benefit from the introduction of retrieval-enhanced prompts. This finding underscores the importance of maintaining a moderate depth for the retrieval-enhanced prompt. While retrieved representations can introduce valuable information, excessive reliance on retrieval can introduce noise.

γ varies. The hyperparameters γ in the guiding loss \mathcal{L} controls the intensity of the retrieval enhancement. As evidenced by the right part of Figure 9, the result continues to improve as γ decreases. These results demonstrate that lower values of γ enhance the reliance on retrieval-enhanced features, leading to significant improvements in classification accuracy. However, for FGVC Aircraft, the highest accuracy is observed at $\gamma = 10^{-1}$, which is caused by its smallest intra-class visual variance.

In summary, the hyper-parameters associated with retrieval critically influence the efficacy of retrieval enhancement. These findings highlight the necessity of striking an optimal balance between incorporating valuable retrieved information and mitigating the potential introduction of noise during the learning process. We provide valuable insights that are instrumental for the design of related methods and establish a guiding framework for future research in this domain.

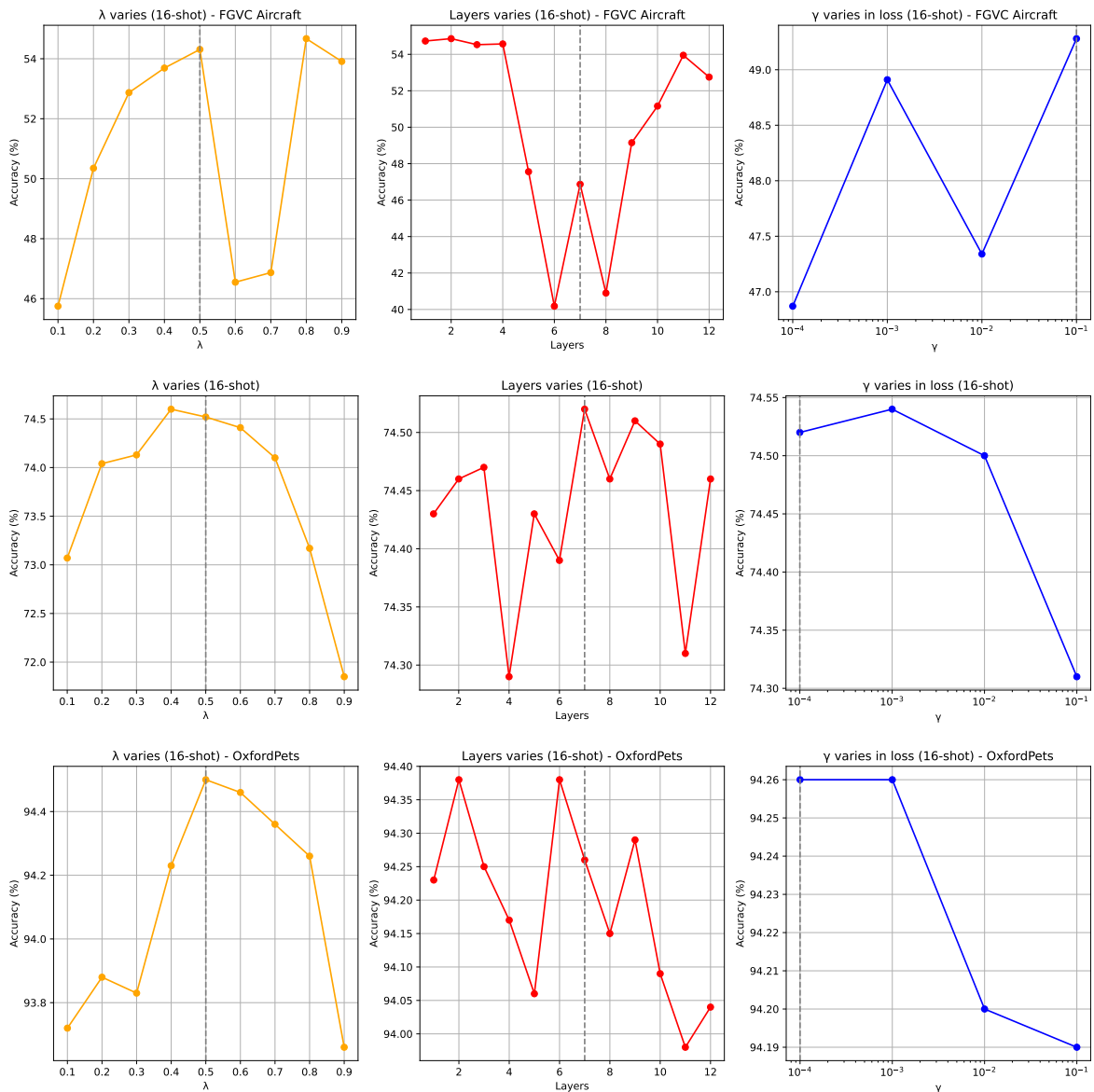


Fig. 9 Tuning retrieval parameter results over 3 datasets under the 16-shot learning setting. From top to bottom, images report ablation experiments about tuning retrieval parameters on FGVC Aircraft, ImageNet, and Oxford Pets, respectively.

7 Conclusion

In this paper, we investigate retrieval-enhanced visual prompt learning for visual-language models. Specifically, we propose integrating the results from a retrieval cache model into model inference using two approaches: prompts and predicted distributions. Additionally, We introduce a prompt learner that dynamically adapts prompts based on retrieval results and an auxiliary classification adapter. To regulate the degree of retrieval enhancement, we introduce the prior distribution obtained from semi-parametric retrieval into the cross-entropy loss to guide prompt tuning.

Extensive experiment results prove that the proposed method achieves superior performance over other prompt-learning methods in few-shot learning and comparable results on domain generalization. More significantly, we extend the RePrompt approach from traditional image datasets to more challenging tasks, including video and multi-view image datasets. Finally, we summarize the relationships between the properties of external memory and retrieval enhancement mechanisms. This conclusion stems from a quantitative analysis of the relationship between the hyperparameters of retrieval enhancement and the data distribution of external memory.

We hope that our findings inspire further research in these promising directions: 1) Extending prompt learning to additional downstream tasks, particularly dense prediction tasks such as semantic segmentation and object detection. 2) Investigating the application of retrieval techniques to address challenges, such as long-tail data. Our study lays the groundwork for future research in enhancing visual-language models through retrieval mechanisms, and we encourage further investigations into these critical areas.

8 Data Availability Statements

The datasets that support the findings of this study are openly available in

- 1) Few-shot image classification: [ImageNet](#), [Caltech101](#), [OxfordPets](#), [StanfordCars](#), [Flowers102](#), [Food101](#), [FGV-CAircraft](#), [SUN397](#), [DTD](#), [EuroSAT](#), [UCF101](#). Download split files from this [link](#)
- 2) Domain generalization task: [ImageNetV2](#), [ImageNet-Sketch](#), [ImageNet-A](#), [ImageNet-R](#).
- 3) Few-shot video understanding: [HMDB51](#), [UCF101](#), [Something Something v2 \(SSv2\)](#), [Kinetics](#)
- 4) Few-shot Multi-few image classification: [MVImgNet](#)

Acknowledgments

This work was supported by National Key R&D Program of China (No. 2022ZD0118700) and Natural Science Foundation of Zhejiang Province (NO. LY21F030018).

References

1. C. Finn, P. Abbeel, and S. Levine, “Model-agnostic meta-learning for fast adaptation of deep networks,” in *ICML*, 2017, pp. 1126–1135.
2. J. Snell, K. Swersky, and R. Zemel, “Prototypical networks for few-shot learning,” *Proc. Adv. Neural Inf. Process. Syst.*, vol. 30, 2017.
3. O. Vinyals, C. Blundell, T. Lillicrap, D. Wierstra *et al.*, “Matching networks for one shot learning,” *Proc. Adv. Neural Inf. Process. Syst.*, vol. 29, 2016.
4. A. Radford, J. W. Kim, C. Hallacy, A. Ramesh, G. Goh, S. Agarwal, G. Sastry, A. Askell, P. Mishkin, J. Clark *et al.*, “Learning transferable visual models from natural language supervision,” in *ICML*, 2021, pp. 8748–8763.
5. C. Jia, Y. Yang, Y. Xia, Y.-T. Chen, Z. Parekh, H. Pham, Q. Le, Y.-H. Sung, Z. Li, and T. Duerig, “Scaling up visual and vision-language representation learning with noisy text supervision,” in *ICML*, 2021, pp. 4904–4916.
6. K. Zhou, J. Yang, C. C. Loy, and Z. Liu, “Learning to prompt for vision-language models,” *Int. J. Comp. Vis.*, vol. 130, no. 9, pp. 2337–2348, 2022.
7. P. Gao, S. Geng, R. Zhang, T. Ma, R. Fang, Y. Zhang, H. Li, and Y. Qiao, “Clip-adapter: Better vision-language models with feature adapters,” *arXiv preprint arXiv:2110.04544*, 2021.
8. C. Ju, T. Han, K. Zheng, Y. Zhang, and W. Xie, “Prompting visual-language models for efficient video understanding,” in *Proc. Eur. Conf. Comp. Vis.*, 2022, pp. 105–124.
9. J. Kirkpatrick, R. Pascanu, N. Rabinowitz, J. Veness, G. Desjardins, A. A. Rusu, K. Milan, J. Quan, T. Rammalho, A. Grabska-Barwinska *et al.*, “Overcoming catastrophic forgetting in neural networks,” *Proceedings of the national academy of sciences*, vol. 114, no. 13, pp. 3521–3526, 2017.
10. M. Toneva, A. Sordoni, R. T. d. Combes, A. Trischler, Y. Bengio, and G. J. Gordon, “An empirical study of example forgetting during deep neural network learning,” *arXiv preprint arXiv:1812.05159*, 2018.
11. M. Jia, L. Tang, B.-C. Chen, C. Cardie, S. Belongie, B. Hariharan, and S.-N. Lim, “Visual prompt tuning,” *arXiv preprint arXiv:2203.12119*, 2022.
12. Y. Zang, W. Li, K. Zhou, C. Huang, and C. C. Loy, “Unified vision and language prompt learning,” *arXiv preprint arXiv:2210.07225*, 2022.
13. M. U. Khattak, H. Rasheed, M. Maaz, S. Khan, and F. S. Khan, “Maple: Multi-modal prompt learning,” *arXiv preprint arXiv:2210.03117*, 2022.
14. Y. Xing, Q. Wu, D. Cheng, S. Zhang, G. Liang, and Y. Zhang, “Class-aware visual prompt tuning for vision-language pre-trained model,” *arXiv preprint arXiv:2208.08340*, 2022.
15. M. U. Khattak, S. T. Wasim, M. Naseer, S. Khan, M.-H. Yang, and F. S. Khan, “Self-regulating prompts: Foundational model adaptation without forgetting,” in *Proceedings of the IEEE/CVF International Conference on Computer Vision*, 2023, pp. 15 190–15 200.
16. A. Long, W. Yin, T. Ajanthan, V. Nguyen, P. Purkait, R. Garg, A. Blair, C. Shen, and A. van den Hengel, “Retrieval augmented classification for long-tail visual recognition,” in *Proc. IEEE Conf. Comp. Vis. Patt. Recogn.*, 2022, pp. 6959–6969.
17. S. Borgeaud, A. Mensch, J. Hoffmann, T. Cai, E. Rutherford, K. Millican, G. B. Van Den Driessche, J.-B. Lespiau, B. Damoc, A. Clark *et al.*, “Improving language models by retrieving from trillions of tokens,” in *ICML*, 2022, pp. 2206–2240.
18. X. Chen, L. Li, N. Zhang, X. Liang, S. Deng, C. Tan, F. Huang, L. Si, and H. Chen, “Decoupling knowledge from memorization: Retrieval-augmented prompt learning,” *arXiv preprint arXiv:2205.14704*, 2022.
19. K. Guu, K. Lee, Z. Tung, P. Pasupat, and M. Chang, “Retrieval augmented language model pre-training,” in *ICML*, 2020, pp. 3929–3938.
20. Z. Yang, W. Ping, Z. Liu, V. Korthikanti, W. Nie, D.-A. Huang, L. Fan, Z. Yu, S. Lan, B. Li *et al.*, “Re-vilm: Retrieval-augmented visual language model for zero and few-shot image captioning,” *arXiv preprint arXiv:2302.04858*, 2023.
21. R. Zhang, W. Zhang, R. Fang, P. Gao, K. Li, J. Dai, Y. Qiao, and H. Li, “Tip-adapter: Training-free adaption of clip for few-shot classification,” in *Proc. Eur. Conf. Comp. Vis.*, 2022, pp. 493–510.
22. Y. Gao, Y. Xiong, X. Gao, K. Jia, J. Pan, Y. Bi, Y. Dai, J. Sun, and H. Wang, “Retrieval-augmented generation for large language models: A survey,” *arXiv preprint arXiv:2312.10997*, 2023.
23. V. Udandarao, A. Gupta, and S. Albanie, “Sus-x: Training-free name-only transfer of vision-language models,” *arXiv preprint arXiv:2211.16198*, 2022.
24. C. Schuhmann, R. Beaumont, R. Vencu, C. Gordon, R. Wightman, M. Cherti, T. Coombes, A. Katta,

- C. Mullis, M. Wortsman *et al.*, “Laion-5b: An open large-scale dataset for training next generation image-text models,” *Advances in Neural Information Processing Systems*, vol. 35, pp. 25 278–25 294, 2022.
25. V. Karpukhin, B. Oğuz, S. Min, P. Lewis, L. Wu, S. Edunov, D. Chen, and W.-t. Yih, “Dense passage retrieval for open-domain question answering,” *arXiv preprint arXiv:2004.04906*, 2020.
 26. N. Kassner and H. Schütze, “Bert-knn: Adding a knn search component to pretrained language models for better qa,” *arXiv preprint arXiv:2005.00766*, 2020.
 27. P. Lewis, E. Perez, A. Piktus, F. Petroni, V. Karpukhin, N. Goyal, H. Küttler, M. Lewis, W.-t. Yih, T. Rocktäschel *et al.*, “Retrieval-augmented generation for knowledge-intensive nlp tasks,” *Proc. Adv. Neural Inf. Process. Syst.*, pp. 9459–9474, 2020.
 28. K. Nakata, Y. Ng, D. Miyashita, A. Maki, Y.-C. Lin, and J. Deguchi, “Revisiting a knn-based image classification system with high-capacity storage,” *arXiv preprint arXiv:2204.01186*, 2022.
 29. U. Khandelwal, O. Levy, D. Jurafsky, L. Zettlemoyer, and M. Lewis, “Generalization through memorization: Nearest neighbor language models,” *arXiv preprint arXiv:1911.00172*, 2019.
 30. R. Zhang, X. Hu, B. Li, S. Huang, H. Deng, Y. Qiao, P. Gao, and H. Li, “Prompt, generate, then cache: Cascade of foundation models makes strong few-shot learners,” in *Proceedings of the IEEE/CVF Conference on Computer Vision and Pattern Recognition*, 2023, pp. 15 211–15 222.
 31. G. Bontempi, H. Bersini, and M. Birattari, “The local paradigm for modeling and control: from neuro-fuzzy to lazy learning,” *Fuzzy sets and systems*, vol. 121, no. 1, pp. 59–72, 2001.
 32. A. Blattmann, R. Rombach, K. Oktay, and B. Ommer, “Retrieval-augmented diffusion models,” *arXiv preprint arXiv:2204.11824*, 2022.
 33. X. L. Li and P. Liang, “Prefix-tuning: Optimizing continuous prompts for generation,” *arXiv preprint arXiv:2101.00190*, 2021.
 34. Y. Lu, J. Liu, Y. Zhang, Y. Liu, and X. Tian, “Prompt distribution learning,” in *Proc. IEEE Conf. Comp. Vis. Patt. Recogn.*, 2022, pp. 5206–5215.
 35. B. Zhu, Y. Niu, Y. Han, Y. Wu, and H. Zhang, “Prompt-aligned gradient for prompt tuning,” *arXiv preprint arXiv:2205.14865*, 2022.
 36. S. Ren, A. Zhang, Y. Zhu, S. Zhang, S. Zheng, M. Li, A. Smola, and X. Sun, “Prompt pre-training with twenty-thousand classes for open-vocabulary visual recognition,” *arXiv preprint arXiv:2304.04704*, 2023.
 37. K. Zhou, J. Yang, C. C. Loy, and Z. Liu, “Conditional prompt learning for vision-language models,” in *Proc. IEEE Conf. Comp. Vis. Patt. Recogn.*, 2022, pp. 16 816–16 825.
 38. B. Lester, R. Al-Rfou, and N. Constant, “The power of scale for parameter-efficient prompt tuning,” *arXiv preprint arXiv:2104.08691*, 2021.
 39. A. Dosovitskiy, L. Beyer, A. Kolesnikov, D. Weissenborn, X. Zhai, T. Unterthiner, M. Dehghani, M. Minderer, G. Heigold, S. Gelly *et al.*, “An image is worth 16x16 words: Transformers for image recognition at scale,” *arXiv preprint arXiv:2010.11929*, 2020.
 40. J. Deng, W. Dong, R. Socher, L.-J. Li, K. Li, and L. Fei-Fei, “Imagenet: A large-scale hierarchical image database,” in *Proc. IEEE Conf. Comp. Vis. Patt. Recogn.*, 2009, pp. 248–255.
 41. R. Rombach, A. Blattmann, D. Lorenz, P. Esser, and B. Ommer, “High-resolution image synthesis with latent diffusion models,” in *Proceedings of the IEEE/CVF conference on computer vision and pattern recognition*, 2022, pp. 10 684–10 695.
 42. J. Johnson, M. Douze, and H. Jégou, “Billion-scale similarity search with gpus,” *IEEE Transactions on Big Data*, vol. 7, no. 3, pp. 535–547, 2019.
 43. T.-Y. Lin, P. Goyal, R. Girshick, K. He, and P. Dollár, “Focal loss for dense object detection,” in *Proc. IEEE Int. Conf. Comp. Vis.*, 2017, pp. 2980–2988.
 44. L. Fei-Fei, R. Fergus, and P. Perona, “Learning generative visual models from few training examples: An incremental bayesian approach tested on 101 object categories,” in *Proc. IEEE Conf. Comp. Vis. Patt. Recogn.*, 2004, pp. 178–178.
 45. O. M. Parkhi, A. Vedaldi, A. Zisserman, and C. Jawahar, “Cats and dogs,” in *Proc. IEEE Conf. Comp. Vis. Patt. Recogn.*, 2012, pp. 3498–3505.
 46. M.-E. Nilsback and A. Zisserman, “Automated flower classification over a large number of classes,” in *2008 Sixth Indian Conference on Computer Vision, Graphics & Image Processing*, 2008, pp. 722–729.
 47. S. Maji, E. Rahtu, J. Kannala, M. Blaschko, and A. Vedaldi, “Fine-grained visual classification of aircraft,” *arXiv preprint arXiv:1306.5151*, 2013.
 48. J. Krause, M. Stark, J. Deng, and L. Fei-Fei, “3d object representations for fine-grained categorization,” in *Proc. IEEE Int. Conf. Comp. Vis.*, 2013, pp. 554–561.
 49. L. Bossard, M. Guillaumin, and L. V. Gool, “Food-101—mining discriminative components with random forests,” in *Proc. Eur. Conf. Comp. Vis.*, 2014, pp. 446–461.
 50. J. Xiao, J. Hays, K. A. Ehinger, A. Oliva, and A. Torralba, “Sun database: Large-scale scene recognition from abbey to zoo,” in *Proc. IEEE Conf. Comp. Vis. Patt. Recogn.*, 2010, pp. 3485–3492.
 51. P. Helber, B. Bischke, A. Dengel, and D. Borth, “Eurosat: A novel dataset and deep learning benchmark for land use and land cover classification,” *IEEE Journal of Selected Topics in Applied Earth Observations and Remote Sensing*, vol. 12, no. 7, pp. 2217–2226, 2019.
 52. M. Cimpoi, S. Maji, I. Kokkinos, S. Mohamed, and A. Vedaldi, “Describing textures in the wild,” in *Proc. IEEE Conf. Comp. Vis. Patt. Recogn.*, 2014, pp. 3606–3613.
 53. K. Soomro, A. R. Zamir, and M. Shah, “Ucf101: A dataset of 101 human actions classes from videos in the wild,” *arXiv preprint arXiv:1212.0402*, 2012.
 54. B. Recht, R. Roelofs, L. Schmidt, and V. Shankar, “Do imagenet classifiers generalize to imagenet?” in *ICML*, 2019, pp. 5389–5400.
 55. H. Wang, S. Ge, Z. Lipton, and E. P. Xing, “Learning robust global representations by penalizing local predictive power,” *Proc. Adv. Neural Inf. Process. Syst.*, vol. 32, 2019.
 56. D. Hendrycks, K. Zhao, S. Basart, J. Steinhardt, and D. Song, “Natural adversarial examples,” in *Proc. IEEE Conf. Comp. Vis. Patt. Recogn.*, 2021, pp. 15 262–15 271.
 57. D. Hendrycks, S. Basart, N. Mu, S. Kadavath, F. Wang, E. Dorundo, R. Desai, T. Zhu, S. Parajuli, M. Guo *et al.*, “The many faces of robustness: A critical analysis of out-of-distribution generalization,” in *Proc. IEEE Int. Conf. Comp. Vis.*, 2021, pp. 8340–8349.
 58. M. Wang, J. Xing, and Y. Liu, “Actionclip: A new paradigm for video action recognition,” *arXiv preprint arXiv:2109.08472*, 2021.

59. B. Ni, H. Peng, M. Chen, S. Zhang, G. Meng, J. Fu, S. Xiang, and H. Ling, "Expanding language-image pre-trained models for general video recognition," in *Proc. Eur. Conf. Comp. Vis.*, 2022.
60. C. Ju, T. Han, K. Zheng, Y. Zhang, and W. Xie, "Prompting visual-language models for efficient video understanding," in *Proc. Eur. Conf. Comp. Vis.*, 2022.
61. H. Rasheed, M. U. Khattak, M. Maaz, S. Khan, and F. S. Khan, "Fine-tuned clip models are efficient video learners," in *Proceedings of the IEEE/CVF Conference on Computer Vision and Pattern Recognition*, 2023, pp. 6545–6554.
62. X. Yu, M. Xu, Y. Zhang, H. Liu, C. Ye, Y. Wu, Z. Yan, C. Zhu, Z. Xiong, T. Liang, G. Chen, S. Cui, and X. Han, "Mvimgnet: A large-scale dataset of multi-view images," in *Proceedings of the IEEE/CVF Conference on Computer Vision and Pattern Recognition (CVPR)*, June 2023, pp. 9150–9161.
63. H. Kuehne, H. Jhuang, E. Garrote, T. Poggio, and T. Serre, "Hmdb: a large video database for human motion recognition," in *Proc. IEEE Int. Conf. Comp. Vis.*, 2011.
64. R. Goyal, S. Ebrahimi Kahou, V. Michalski, J. Materzynska, S. Westphal, H. Kim, V. Haedel, I. Freund, P. Yianilos, M. Mueller-Freitag *et al.*, "The" something something" video database for learning and evaluating visual common sense," in *Proc. IEEE Int. Conf. Comp. Vis.*, 2017.
65. L. Wang, Y. Xiong, Z. Wang, Y. Qiao, D. Lin, X. Tang, and L. Van Gool, "Temporal segment networks: Towards good practices for deep action recognition," in *Proc. Eur. Conf. Comp. Vis.*, 2016.
66. W. Kay, J. Carreira, K. Simonyan, B. Zhang, C. Hillier, S. Vijayanarasimhan, F. Viola, T. Green, T. Back, P. Natsev *et al.*, "The kinetics human action video dataset," *arXiv preprint arXiv:1705.06950*, 2017.
67. A. Radford, J. W. Kim, C. Hallacy, A. Ramesh, G. Goh, S. Agarwal, G. Sastry, A. Askell, P. Mishkin, J. Clark *et al.*, "Learning transferable visual models from natural language supervision," in *International conference on machine learning*. PMLR, 2021, pp. 8748–8763.
68. S. Hochreiter and J. Schmidhuber, "Long short-term memory," *Neural computation*, vol. 9, no. 8, pp. 1735–1780, 1997.
69. H. Sak, A. W. Senior, and F. Beaufays, "Long short-term memory recurrent neural network architectures for large scale acoustic modeling," in *INTERSPEECH*, 2014, pp. 338–342.